

# RSC Advances



This is an *Accepted Manuscript*, which has been through the Royal Society of Chemistry peer review process and has been accepted for publication.

*Accepted Manuscripts* are published online shortly after acceptance, before technical editing, formatting and proof reading. Using this free service, authors can make their results available to the community, in citable form, before we publish the edited article. This *Accepted Manuscript* will be replaced by the edited, formatted and paginated article as soon as this is available.

You can find more information about *Accepted Manuscripts* in the [Information for Authors](#).

Please note that technical editing may introduce minor changes to the text and/or graphics, which may alter content. The journal's standard [Terms & Conditions](#) and the [Ethical guidelines](#) still apply. In no event shall the Royal Society of Chemistry be held responsible for any errors or omissions in this *Accepted Manuscript* or any consequences arising from the use of any information it contains.



## Preparation, characterization and long-term antibacterial activity of Ag-poly(dopamine)-TiO<sub>2</sub> nanotubes composites

Hongfen Wang<sup>†,a,\*</sup>, Luyao Wei<sup>†,a</sup>, Zhiqi Wang<sup>b</sup> and Shougang Chen<sup>a,\*</sup>

Received 21th October 2015,  
Accepted 00th January 20xx

DOI: 10.1039/x0xx00000x

www.rsc.org/

A simple and efficient approach for the loading of Ag nanoparticles on the poly(dopamine)-modified TiO<sub>2</sub> nanotubes (PDA-TNTs) was used to prepare Ag nanoparticles-poly(dopamine)-TiO<sub>2</sub> nanotubes composite (Ag-PDA-TNTs) that was applied as a long-term antibacterial agent to inhibit the growth of bacterial cells. The features of the obtained Ag-PDA-TNTs were investigated by TEM, XRD, FT-IR and XPS analysis. Anatase TNTs were encapsulated in PDA layers with thickness of about 3 nm on which about 20.4 wt% of single crystalline Ag nanoparticles anchored. XPS and FT-IR results indicated that the PDA layer not only served as a reduction reagent that could reduce Ag<sup>+</sup> ions to Ag nanoparticles but also worked as an adhesive coating by tethering the Ag nanoparticles on the surface of PDA-TNTs. The long-term release profiles of the nanocomposites showed that PDA layers slowed the release rate of Ag nanoparticles, implying the possible long-term antibacterial activity of Ag-PDA-TNTs; and the antibacterial assays verified this point. Besides that, the antibacterial activity of Ag-PDA-TNTs under visible light was higher than that in the dark because of the synergistically antibacterial effects of Ag nanoparticles and ROS under visible light irradiation. Compared with the antibacterial activity of TiO<sub>2</sub> nanotubes loaded with Ag nanoparticles (Ag-TNTs), Ag-PDA-TNTs had higher and longer-term antibacterial activity which owned to the effect of PDA layers by tethering Ag nanoparticles on TNTs and slowing Ag<sup>+</sup> ions release rate. This work provides a new method for the preparation of Ag-based antibacterial agents and facilitates their practical application in modern antifouling and biomedical fields.

### 1. Introduction

As the most frequently studied photocatalysis material, anatase TiO<sub>2</sub> has been proposed as one of the best disinfection materials as it can degrade bacteria to harmless small molecules such as H<sub>2</sub>O, CO<sub>2</sub>.<sup>1,2</sup> The electrons and holes induced by light excitation have strong oxidizing activities, and subsequently react with water and oxygen molecules (H<sub>2</sub>O and O<sub>2</sub>) to yield reactive oxygen species (ROS), such as hydroxyl radicals ( $\cdot\text{OH}$ ), superoxide anions ( $\text{O}_2^{\cdot-}$ ), and hydrogen peroxide (H<sub>2</sub>O<sub>2</sub>),<sup>3</sup> which are strong oxidants not only for toxic organic molecules but also for bacteria.<sup>4-6</sup> However, there are still drawbacks of the wide band gap that only responses to a narrow light-absorption range (only 3-5% of the solar spectrum) and high recombination of electron-holes, which result in the slow reaction rate and little effect of illumination on bacteria.<sup>7</sup>

To improve the antibacterial activity of TiO<sub>2</sub>, various studies have been carried out. In particular, Ag-based TiO<sub>2</sub> gains intense attention for its improvement of photocatalytic reactions and antibacterial activity under visible light

irradiation,<sup>8,9</sup> commonly in the form of Ag<sup>+</sup> ions and metallic Ag. Although the antibacterial activities of Ag ions at a low concentration has been confirmed for a long time, however, Ag nanoparticles nowadays are more highly favorable owing to their low biotoxicity, high disinfection efficiency, good stability, long-term antibacterial activity, and so on.<sup>10</sup> Ag nanoparticles can exert an excellent antibacterial activity through a multifactorial process which involving either damaging of bacterial cell walls and plasma membrane, or inhibition of DNA replication and protein synthesis.<sup>11</sup> Moreover, it has been demonstrated that the surface plasma resonance of Ag nanoparticles can greatly improve the photocatalytic antibacterial activity of TiO<sub>2</sub> by enhancing the electron-hole separation and extending the light-absorption range of TiO<sub>2</sub> into the visible region.<sup>12,13</sup> Furthermore, it has been recently confirmed that a sufficient loading amount of Ag nanoparticles could boast a relatively long-term antibacterial ability of Ag-based TiO<sub>2</sub>.<sup>14</sup> Although Ag-based TiO<sub>2</sub> nanoparticles have been extensively investigated in the medical fields, however, the limitation of the relatively low surface area of TiO<sub>2</sub> particles makes it difficult to load a large amount of Ag nanoparticles, which restricts the long-term antibacterial activity.<sup>15-16</sup> Compared with TiO<sub>2</sub> particles, TiO<sub>2</sub> nanotubes (TNTs) possess unique properties including higher specific surface area, stronger adsorption ability and more favorable bioactivity; therefore they exhibit good application prospect in modern antifouling and biomedical fields.<sup>17</sup> Not

<sup>a</sup> Institute of Material Science and Engineering, Ocean University of China, Qingdao, 266100, China. Email: wanghongfen11@163.com; sgchen@ouc.edu.cn.

<sup>b</sup> Qingdao Institute of Bioenergy and Bioprocess Technology, Chinese Academy of Sciences, Qingdao, 266101, China.

<sup>c</sup> † These authors contributed equally to the work.

only the hollow structure of TNTs makes them can serve as nanocontainers to store a large amount of antibacterial agents, but also their unique “open-ended” nanostructure and large length-diameter ratio make it feasible for controlling the release of these drugs, thus producing sustained antibacterial effects. Many reports have investigated the loading of Ag nanoparticles into TNTs arrays prepared by anodization on Ti foils and confirmed the efficiently antibacterial property,<sup>18-19</sup> however, the weak van der Waals interactions between Ag nanoparticles and TNTs can easily cause the problem of burst Ag release in the early stage of application, thus inevitably weakens or even totally loses their antibacterial activities.<sup>19</sup> Therefore, modification of the interface of TNTs and Ag nanoparticles is highly desirable to ensure large loading amount of Ag and achieve sustained release patterns for the prolonged antibacterial period.

As an eco-friendly biopolymer, dopamine is widely used in surface modification for its self-polymerization on foreign substrates and adhering on nearly any inorganic and organic surfaces through the formation of strong covalent and noncovalent bonds with these surfaces. At the same time, the formed polydopamine (PDA) coating can serve as a versatile platform for secondary reactions, leading to tailoring of coatings in material synthesis, drug release, sensors, and immunoassays.<sup>20,21</sup> In such a way, PDA can be used as a binder to integrate TNTs and Ag nanoparticles tightly and stably, forming a three-in-one nanocomposite with excellent antibacterial activity.

In this work, PDA layers were prepared on TNTs and used as media that possessed reducing ability and stabilizing ability for the loading of Ag nanoparticles on TNTs. The numerous amine and catechol functional groups in PDA were exploited to absorb Ag<sup>+</sup> ions by metal-binding ability and reduce them into Ag nanoparticles by its weak reducibility. The preparation process was eco-friendly and easily operated, thus a large quantity of PDA interface-modified Ag-TNTs (Ag-PDA-TNTs) were obtained. The Ag-PDA-TNTs were characterized with transmission electron microscopy (TEM), X-ray diffractometry (XRD), Fourier transfer infrared spectroscopy (FTIR) and X-ray photoelectron spectroscopy (XPS) analysis to verify the effect of PDA layers and the growth of Ag nanoparticles on PDA-TNTs. The release behaviour of Ag was explored to study the effect of PDA interface-modification between TNTs and Ag nanoparticles. Antibacterial assays were conducted with agar diffusion method to investigate the long-term antibacterial activity of Ag-PDA-TNTs with *Escherichia coli* (*E. coli*) and *Staphylococcus aureus* (*S. aureus*) as model microbes.

## 2. Experimental

### 2.1. Materials

Dopamine hydrochloride was purchased from Alfa Aesar. Sodium hydroxide (NaOH), silver nitrate (AgNO<sub>3</sub>) were purchased from Sinopharm Chemical Reagent Co.. Anatase TNTs as a starting material were synthesized using an alkali-hydrothermal method, and more details of this method are

given in our previous work.<sup>22</sup> Phosphate buffer solution (PBS) was prepared by adjusting the ratio of 0.1 mol/l Na<sub>2</sub>HPO<sub>4</sub> and 0.1 mol/l KH<sub>2</sub>PO<sub>4</sub>. All other chemicals used in this study were of analytical grade and used as received without further purification.

### 2.2. Preparation of PDA-TNTs

PDA modification of TNTs was conducted as the follows process. TNTs were initially dispersed in a beaker containing 200 ml of deionized water. Following that, 50 mg of dopamine hydrochloride were added, and the transparent suspension immediately turned into orange. The pH value of the mixture was adjusted to 8.5 with 2 mol/l NaOH solution, and the reaction was maintained under magnetic stirring for 8 h. The color of the mixture gradually became dark brown with the stirring time increased. After the reaction, the precipitant was collected and rinsed with distilled water until Cl<sup>-</sup> ions were removed completely. Finally, the product was dried at 80 °C in a vacuum oven and some dark brown particles were obtained.

### 2.3 Preparation of Ag-PDA-TNTs

PDA-TNTs were dispersed uniformly in 0.1 mol/l AgNO<sub>3</sub> solution in the dark with magnetic stirring for 4 h at 40 °C. The mixture was then put into a vacuum oven by controlling 0.05 MPa pressure for 1 h, assuring more Ag<sup>+</sup> ions were absorbed on PDA-TNTs. During this process, most of Ag<sup>+</sup> ions could be reduced to Ag nanoparticles with the aid of weak reducibility of PDA and anchored on PDA-TNTs.<sup>23</sup> The suspension was centrifuged and some dark precipitants were collected. To assure the absorbed Ag<sup>+</sup> ions on PDA-TNTs surface to be reduced to Ag nanoparticles completely, the wet Ag-PDA-TNTs were then irradiated by 500 W ultraviolet lights for 0.5 h, and dried at 80 °C in a vacuum oven. For comparison, Ag-TNTs with brown color were also obtained by photo-reduction method, and the preparation procedure was the same as that of Ag-PDA-TNTs.

### 2.4 Characterization

The crystal structure of the samples was determined by X-ray diffractometer (D8, Bruker, Germany) with Cu K $\alpha$  radiation ( $\lambda=0.15405$  nm) with a step size of 0.02°. To determine the microstructure and the size of Ag nanoparticles, high-resolution transmission electron microscopy and corresponding selected area electron diffraction (HRTEM/SAED) were performed on a transmission electron microscope (JEM-2100, JEOL, Japan). The surface-chemistry of different samples was analyzed using the Fourier transform infrared spectroscope (IS50, Thermo Fisher, USA) within the frequency range of 400-4500 cm<sup>-1</sup>. The chemical composition of the samples was determined by X-ray photoelectron spectroscopy (XPS, ESCALAB 250Xi, Thermo Fisher, USA) with monochromated Al K $\alpha$  radiation (1486.6 eV).

### 2.5 Silver release behaviour

To compare the Ag release behaviour of Ag-TNTs with that of Ag-PDA-TNTs, the 50-day Ag release profiles of the samples were investigated. 0.5 g of Ag-TNTs and Ag-PDA-TNTs were respectively dispersed in 25.0 ml phosphate buffered saline (PBS) solutions (pH = 8) by ultrasonication, and then the suspensions were kept in a digital shaking air bath at 37 °C. The samples were taken out at a predetermined time interval, and then were dialyzed with dialysis bags. The concentration of Ag in dialysate was detected by inductively coupled plasma mass spectrometry (ICP-Q, Thermo Fisher, USA), and the precipitates were collected to determine the antibacterial activity of Ag-based TNTs from which Ag released. Each sample was performed in triplicate and the results were expressed as the mean.

### 2.6 Antibacterial assay

The persistent antibacterial activity of the Ag-based TNTs that were immersed in PBS for different time was studied by agar diffusion method against *E. coli* (ATCC 25922), and *S. aureus* (ATCC 25923), which were selected as models for gram-negative bacteria and gram-positive bacteria, respectively. The bacteria were activated with LB broth and diluted with fresh LB broth before the antibacterial assay. In the tests, 0.5 ml suspensions of the activated bacteria were spread onto agar plates, and several circular filter papers with diameter of 15 mm soaked in antibacterial agents suspensions (200 mg/l) were lightly placed on top of the inoculated agar plates and incubated at 37 °C with or without visible light irradiation, to evaluate the effect of the light irradiation on antibacterial activity of Ag-based TNTs. After incubation at 37 °C over night, pictures of the agar plates were captured. The long-lasting antibacterial activities of the Ag-based TNTs were evaluated according to the change of diameters of the inhibition zones. Each sample was performed in triplicate in the antibacterial experiments and the typical images were used.

## 3. Results and discussion

### 3.1 TEM analysis

To investigate the nanostructures of the as-prepared products, the typical TEM images of them were firstly observed, shown in Fig. 1. According to Fig. 1a and d, the TNTs with length of 50-200 nm showed open-end tubular nanostructures that were extremely beneficial for the loading of Ag ions, and the outer and inner diameters were 9-10 nm and 5-6 nm, respectively. After being surface-modified with PDA, a rough PDA layer with thickness of about 3 nm on the TNTs was observed in Fig. 1e. In addition, the TNTs were top-sealed by the PDA layer that might hamper Ag nanoparticles diffusing into the cavity of TNTs. However, although the surface of TNTs was covered with some black dots (Fig. 1b) after the loading of Ag nanoparticles, the same as PDA-TNTs (Fig. 1c), it was found that the density of the black dots anchored on TNTs was much lower than that on PDA-TNTs by comparing the HRTEM images of Ag-TNTs (Fig. 1f) with that of Ag-PDA/TNTs (Fig. 1g). This phenomenon indicated that the PDA layer could increase the

loading amount of Ag nanoparticles on TNTs, and this inference would be verified by the next measurements. HRTEM images and the corresponding SAED patterns were obtained to characterize the crystalline nature of Ag-PDA/TNTs (Fig. 2). Two sets of diffraction patterns could be observed: the single crystal diffraction spot and the polycrystalline rings, which corresponded to Ag nanoparticles and TNTs, respectively.<sup>24</sup> From Fig. 2a and c, it was revealed that the attached Ag nanoparticles possessed a single-crystalline nature, and the lattice fringes arranging along one direction with interplanar distances of 0.234 nm, 0.202nm, 0.121nm and 0.141nm were consistent with the (111), (200) (311) and (220) planes of cubic Ag, respectively.<sup>25</sup> However, it was concluded from Fig. 2b and d that the TNTs consisted of lots of nanocrystals randomly arranged and yielded a polycrystalline structure, and the interplanar distances of the fringes were 0.348 nm and 0.185nm, corresponding to (101) and (200) planes of anatase TiO<sub>2</sub>.

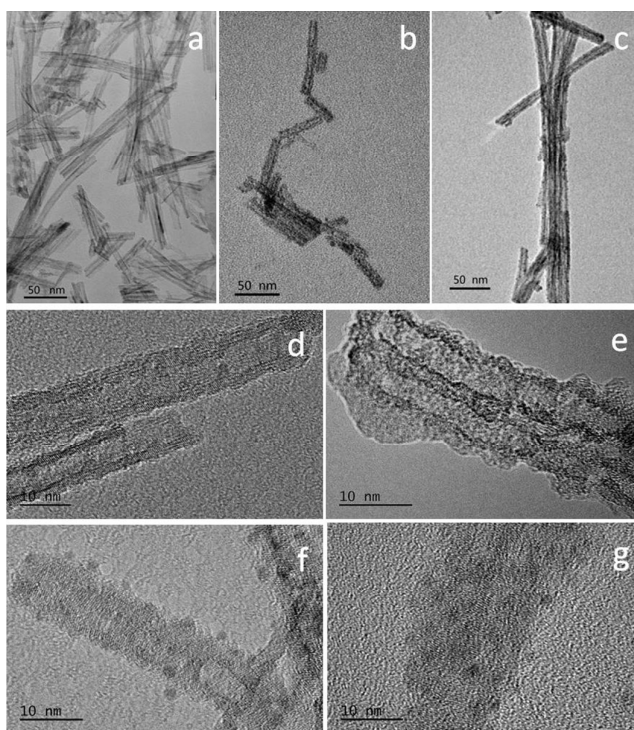


Fig. 1 TEM images of (a) TNTs, (b) Ag-TNTs, (c) Ag-PDA-TNTs; and HR-TEM images of (d) TNTs, (e) PDA-TNTs, (f) Ag-TNTs, (g) Ag-PDA-TNTs.

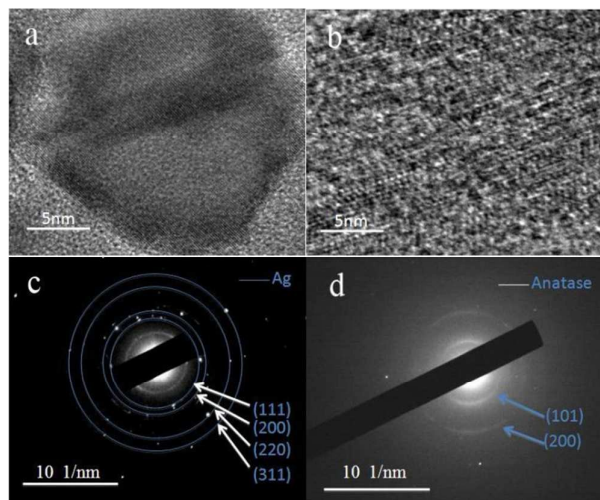


Fig. 2 HRTEM images of (a) Ag and (b) TNTs and the corresponding SAED patterns of (c) Ag and (d) TNTs on Ag-PDA/TNTs.

### 3.2 XRD analysis

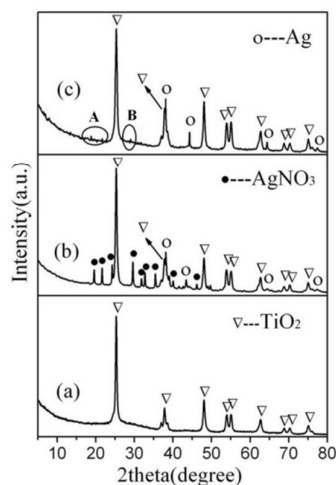


Fig. 3 XRD patterns of (a) TNTs, (b) Ag-TNTs and (c) Ag-PDA-TNTs.

To further verify the successful synthesis of Ag-PDA-TNTs and Ag-TNTs, XRD measurement was conducted. Fig. 3 showed the XRD patterns of TNTs, Ag-TNTs and Ag-PDA-TNTs, curves a, b and c, respectively. All diffraction peaks in Fig. 3a were indexed to the anatase  $\text{TiO}_2$  (JCPDS21-1272), which had a favorable structure for  $\text{Ag}^+$  ions being photo-reduced to Ag nanoparticles. From the XRD pattern of Ag-TNTs, it can be found that the diffraction peaks of  $\text{AgNO}_3$  (JCPDS43-0649) and the face-centered cubic Ag crystals (JCPDS65-2871) both appeared in Fig. 1b, and this was related to a fact that only a

part of  $\text{Ag}^+$  ions were reduced to metallic Ag nanoparticles during the process of ultraviolet light radiation. However, in the XRD pattern of Ag-PDA-TNTs, shown in Fig. 3c, all the main diffraction peaks were indexed to the face-centered cubic Ag crystals (JCPDS65-2871) except the diffraction peaks of anatase TNTs. Besides that, the weak diffraction peaks located at Fig. 3c-A and Fig. 3c-B were similar to that of  $\text{AgNO}_3$  but with lower angle diffraction, which implied larger lattice-plane spacing. Compared the diffraction peaks in Fig. 3b with that in Fig. 3c, it was obvious that the intensity of the diffraction peaks of Ag crystals presented in Ag-PDA-TNTs were stronger than that in Ag-TNTs, and this implied that the amount of Ag crystal loaded on PDA-TNTs was much more than that on Ag-TNTs. According to the results of quantitative analysis using Rietveld whole pattern fitting method, Ag-TNTs were composed of 6.1 wt% of Ag nanoparticles, 17.2 wt% of  $\text{AgNO}_3$ , and Ag-PDA-TNTs were composed of 20.4 wt% of Ag nanoparticles, 3.2 wt% of  $\text{AgNO}_3$ . The molar ratio of Ag atoms to Ti atoms was about 1:6 in Ag-TNTs, while that of Ag-PDA-TNTs was about 1:4.5. Therefore, it could be deduced that the existence of PDA on TNTs were in favor of the absorption of  $\text{Ag}^+$  ions and increased the loading amount of Ag nanoparticles on TNTs, which was in agreement with the result in literatures.<sup>24</sup>

### 3.3 FT-IR analysis

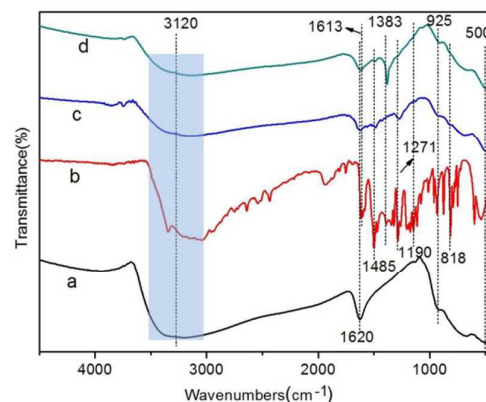


Fig. 4 FT-IR spectra of (a) TNTs, (b) PDA, (c) PDA-TNTs and (d) Ag-PDA-TNTs.

FT-IR characterization was carried out to further ascertain the chemical structure of the Ag-PDA-TNTs. The characteristic FT-IR spectra of TNTs, PDA, PDA-TNTs and Ag-PDA-TNTs were displayed in Fig. 4, curves a-d, respectively. In all four curves, the broad absorption from 3600 to 3100  $\text{cm}^{-1}$  was attributed to the O–H stretching vibration on the surface of the materials.<sup>26</sup> In Fig. 4a, the characteristic absorption band of  $\text{TiO}_2$ , identified with Ti–O–Ti stretching vibration at about 500  $\text{cm}^{-1}$  emerged. As shown in the FT-IR spectrum of PDA (Fig. 4b), the peaks at 1613  $\text{cm}^{-1}$  and 1485  $\text{cm}^{-1}$  were ascribed to C=C stretching vibration of indole and benzenoid rings, respectively.<sup>27,28</sup> The peaks at 1383  $\text{cm}^{-1}$  and 1271  $\text{cm}^{-1}$  were assigned to C–N stretching or bending vibrations and –C=N

stretching vibration of amide, respectively;<sup>29</sup> Some other peaks at 600-900  $\text{cm}^{-1}$  (out-of-plane bending vibration of benzene ring), the peaks around 2875  $\text{cm}^{-1}$  (C-H asymmetric in the CH and  $\text{CH}_2$  groups of benzene ring), 1720  $\text{cm}^{-1}$  (O=C=O) and 1190  $\text{cm}^{-1}$  (C-O-H), etc. also emerged in the FT-IR spectrum of PDA, indicating that PDA could be synthesized in the current condition. However, in the FTIR spectra of the PDA-TNTs and Ag-PDA-TNTs, not only the peaks representing the groups of C-H, O=C=O, C-N, -C=N and C-O-H decreased in intensity, but their location also shifted, from which we speculated that PDA was successfully deposited on the surface of the TNTs with the aid of metal-binding ability of catechol and nitrogen-containing groups present in the PDA structure. Furthermore, by comparing Fig. 4c with Fig. 4d, it was found that the peaks intensity of -C=N decreased while that of C-N increased, and it indicated that -C=N might turn into C-N with the loading of Ag nanoparticles, which lowered the energy of system made it more stable.<sup>30</sup>

### 3.4 XPS analysis

To gain further insight into the features of Ag-PDA-TNTs, XPS was performed on Ag-PDA-TNTs to confirm not only chemical status of the elements but also the interaction between Ag, Ti and PDA. Low resolution survey spectra was shown in Fig. 5a, yielding peak positions for Ti, O, C, N and Ag which were the characteristic elements of Ag-PDA-TNTs. A high-resolution scan of Ti 2p (Fig. 5b) was composed of two peaks of  $\text{Ti } 2p_{3/2}$  and  $\text{Ti } 2p_{1/2}$  at the binding energies (BE) of 458.6 and 464.4 eV, which were in good agreement with the  $\text{Ti}^{4+}$  state.<sup>31</sup> As for the high-resolution scan of O 1s (Fig. 5c), there were four peak components: at a BE of 29.6, 530.4 eV for Ti-O species, at a BE of 531.3 eV for C=O/C-O...Ti species, at a BE of 532.2 eV for Ti-OH species. However, there was no C-OH peak at 533.5 eV because of the formation of coordination bond (C-O...Ti) by the deprotonation of C-OH groups upon  $\text{TiO}_2$  binding, and this further confirmed the formation of coordination bond (C-O...Ti), implying that there were binding force between TNTs and PDA membrane. In Fig. 5d, the main peak of C 1s was resolved into four peaks at 284.6 eV (C-C/C-H), 285.4 eV (C-N in Py rings), 286.2 eV (C-O) and 288.4 eV (C=N), 291.6 eV ( $\pi$ - $\pi^*$ ), respectively.<sup>32-34</sup> Similarly, the main peaks of N 1s consisted of a imine (=N-R) peak at a BE of 398.8 eV, a secondary (R-NH-R) peak at a BE of 399.9 eV, a primary (R-NH<sub>2</sub>) peak at a BE of 400.8 eV and a protonated (R-NH<sub>3</sub><sup>+</sup>) peak at a BE of 401.7 eV, shown in Fig. 5e.<sup>35</sup> The presence of these amine functionalities showed the successful formation of a PDA layer on the surface of TNTs and provided an opportunity for  $\text{Ag}^+$  ions to form -NH<sub>2</sub> ligands. In the high-resolution scan of Ag 3d (Fig. 5f), two obvious peaks centered at the binding energy of 368.3 and 374.3 eV were ascribed to  $\text{Ag } 3d_{5/2}$  and  $\text{Ag } 3d_{3/2}$ , respectively. The peak positions observed here were slightly larger than the expected for metallic  $\text{Ag}^0$  ( $\text{Ag } 3d_{5/2}$ , 367.4 eV and  $\text{Ag } 3d_{3/2}$ , 373.4 eV) while smaller than the  $\text{Ag}^+$  ion ( $\text{Ag } 3d_{5/2}$ , 369.4 eV and  $\text{Ag } 3d_{3/2}$ , 375.6 eV).<sup>36,37</sup> The difference might be a consequence of Ag nanoparticles encapsulated in the organic network and  $\text{Ag}^+$  ions forming

coordination compounds with PDA with the aid of the amine groups,<sup>36</sup> as was consistent with the analysis result of Fig. 3.

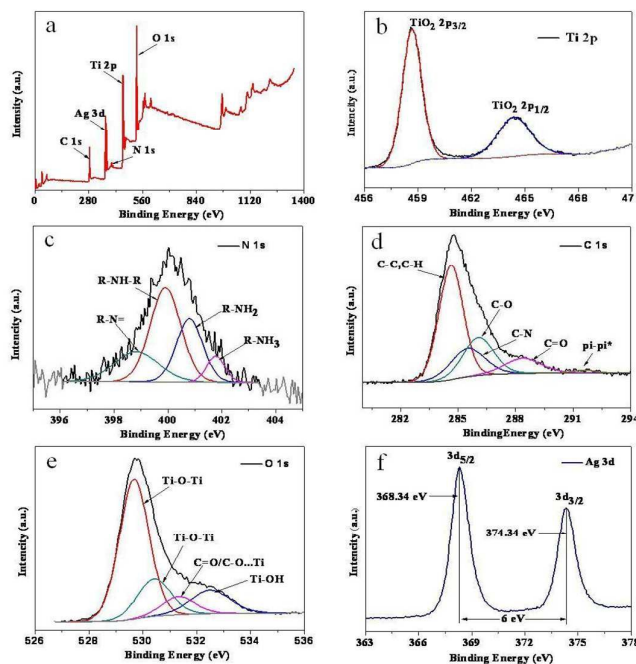


Fig. 5 XPS spectra of Ag-PDA-TNTs: (a) the survey scan and the high resolution scan of (b) Ti 2p, (c) N 1s, (d) C 1s, (e) O 2s, (f) Ag 3d.

### 3.5 Ag release test

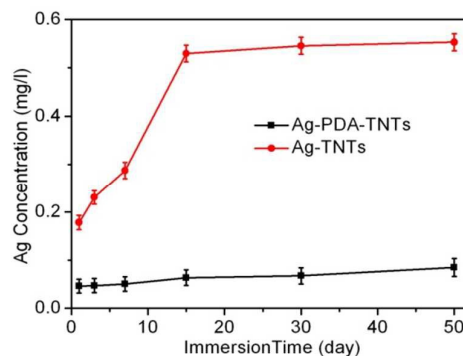


Fig. 6 Ag release profiles of Ag-PDA-TNTs and Ag-TNTs in PBS during 50 days of immersion.

The effect of surface-modification with PDA on Ag release for TNTs was given in Fig. 6. It is known that the antibacterial effect of fungicides weakens with the release of effective ingredients from them.<sup>39</sup> As for the Ag-TNTs immersed in phosphate buffer solution (PBS), the concentration of released Ag in PBS rose faster with time in the first several days, and then reached a near steady-state after 14 days, which implied that Ag-TNTs went into a slowly sustainable Ag release

process. However, the Ag release from Ag-PDA-TNTs underwent a relatively steady process from the beginning to the end of the experiment, although the concentration of released Ag in PBS



Fig. 7 Diffusion inhibition zones of the (1) blank, (2) Ag-PDA-TNTs and (3) Ag-TNTs that were immersed in PBS for different time (0d, 1d, 3d, 7d, 15d, 30d, 50d) without visible light irradiation against *E. coli* (a-g) and *S. aureus* (h-n)/with visible light irradiation against *E. coli* (A-G) and *S. aureus* (H-N).

Table 1 Diameters of the inhibition zones of Ag-PDA-TNTs and Ag-TNTs that were immersed in PBS for different time against different bacteria with/without visible light irradiation

Immersion time	Diameters of the inhibition zones /mm							
	E.coli /light		S.aureus/light		E.coli/ without light		S.aureus/without light	
	APT	AT	APT	AT	APT	AT	APT	AT
0 day	20.4	19.2	21.3	20.6	19.9	18.9	20.1	18.6
1 day	19.8	18.2	21.1	19.5	19.5	17.9	19.6	18.3
3 days	19.6	18.0	19.6	18.7	18.9	17.5	19.3	17.8
7 days	19.3	18.0	19.3	18.8	18.0	17.4	19.2	17.4
15 days	18.9	17.8	19.0	17.8	17.3	16.9	18.9	17.1
30 days	17.6	16.5	18.5	17.4	16.3	16.1	17.2	16.0
50 days	17.1	16.2	17.6	16.7	16.4	15.8	16.9	16.1

increased very slowly. Unlike the Ag release profile of Ag-TNTs, there was no burst release in the Ag release profile of Ag-PDA-TNTs. Compared Ag release profile of Ag-PDA-TNTs with that of Ag-TNTs, the concentration of Ag released from Ag-PDA-TNTs in PBS was far lower than that from Ag-TNTs, which indicated that the surface-modification with PDA was in favor of the controllable Ag release from TNTs, thus assured the long-term antibacterial activity of Ag-PDA-TNTs.

### 3.6 Antibacterial assay

Antibacterial behaviour of Ag-PDA-TNTs and Ag-TNTs that were immersed in PBS for different time were evaluated by

agar diffusion method (Fig. 7). All samples showed good response against *E. coli* and *S. aureus*, even for Ag-PDA-TNTs/Ag-TNTs immersed in PBS for 50 days, which showed a long-term antibacterial activity had been achieved by a sustained Ag release. To clearly interpret the change of antibacterial activity, the diameters of inhibition zones were measured and presented in Table 1. It is understandable that the greater is the diameter for inhibition zone; the better is the antibacterial activity of an antibacterial agent. From table 1, it was easily to find that with immersion time increasing, both Ag-PDA-TNTs and Ag-TNTs displayed slightly reduced diameters of inhibition zones against *E. coli* (E.C) and *S. aureus*

(S.A). These reduced diameters of inhibition zones were related to the reduced amount of Ag on these samples as Ag released slowly from Ag-PDA-TNTs/Ag-TNTs into PBS. That was to say, the loading amount of Ag on Ag-PDA-TNTs/Ag-TNTs decreased with immersion time increasing in PBS, as was in good accordance with the results of Ag release analysis, and this finally caused the reduction of Ag contribution in inhibition of bacterial growth and weakened the effect of killing bacteria. However, compared with Ag-TNTs that were immersed for the same time in PBS, Ag-PDA-TNTs showed wider inhibition zones that might be due to their larger Ag contents.<sup>40</sup> This result was consistent with the previous analysis, and at the same time demonstrated that PDA layer on TNTs could delay the release rate of Ag nanoparticles, thus attaining a prolonged antibacterial activity for Ag-PDA-TNTs. Moreover, whether in case of Ag-PDA-TNTs or Ag-TNTs that were immersed for the same time in PBS, the inhibition zones against *S. aureus* (gram-positive) were always wider than that against *E. coli* (gram-negative), and this phenomenon was attributed to the different structure of the cell walls of bacteria. It was generally accepted that the antibacterial activities were realized by the interaction between nanoparticles and bacteria occurs through initial adhesion, accumulation of nanoparticles on the bacterial cell wall, alteration/perforation of the cell wall and finally penetration of nanoparticles inside the cell leading to cell death. Since the cell wall of the gram-positive bacteria consisted of a thick layer of peptidoglycan, and nanoparticles were more easily adhesive to the cell walls of gram-positive bacteria and penetrated into the cells than what they did on the gram-negative bacteria whose cell walls with complicatedly multi-layered structure, thus causing larger increases in membrane permeability.<sup>40,41</sup> Just because of this, the inhibition zones of Ag-PDA-TNTs/Ag-TNTs against *S. aureus* were wider than *E. coli*. According to literatures,<sup>42,43</sup> Ag nanoparticles under light irradiation would produce reactive oxygen species (ROS) in the vicinity of the bacterial cell membrane which led to the cell permeability and hence cell death, the higher antibacterial activity of Ag-PDA-TNTs/Ag-TNTs under light irradiation should be attained by comparing with those without light irradiation. As was verified in table 1, the diameters of the inhibition zones of the specimens with the light irradiation were wider than those specimens with the same antibacterial agent without light irradiation, implying the synergistically antibacterial effect of Ag nanoparticles and ROS.

#### 4. Conclusion

Ag-PDA-TNTs with a large quantity were successfully prepared by an easily operated method, where Ag<sup>+</sup> ions were reduced by combining in situ reduction and photo-reduction methods, and the features were analyzed by techniques such as XRD, HR-TEM, FT-IR and XPS. The PDA layers with thickness of about 3nm not only worked as the chemisorptions and reduction sites for Ag<sup>+</sup> ions, but also stabilized and delayed the release rate of the thus formed Ag nanoparticles, thus made Ag-PDA-TNTs attain a long-term antibacterial activity. The as-prepared

Ag-PDA-TNTs had better antibacterial effect against *S. aureus* than *E. coli*, and the antibacterial activity under visible light was higher than that in the dark which due to the synergistically antibacterial effect of Ag nanoparticles and ROS. In comparison with Ag-TNTs, Ag-PDA-TNTs exhibited lower level of Ag release rate and higher antibacterial activity, demonstrating the high loading density of Ag nanoparticles and the long-term antibacterial effects of Ag-PDA-TNTs. Such products could have promising application as antibacterial materials for microbicides and implant devices.

#### Acknowledgments

We greatly acknowledge the financial support from the Doctoral Foundation of Shandong Province (BS2013CL014) and National Natural Science Foundation of China (21203171; 51302254).

#### Reference

- [1] A.A. Ashkarran, S.M. Aghigh, M. kavianipour, N.J. Farahani, *Curr. Appl. Phys.*, 2011, 11, 1048.
- [2] F. Liu, H. Liu, X. Li, H. Zhao, D. Zhu, Y. Zheng, C. Li, *Appl. Surf. Sci.*, 2012, 258, 4667.
- [3] E. M. Rodríguez, G. Márquez, M. Tena, P.M. Álvarez, F.J. Beltrán, *Appl. Catal. B: Environmental*, 2015, 178, 44.
- [4] A. Markowska-Szczupak, K. Ulfig, A.W. Morawski, *Catal. Today*, 2011, 169, 249.
- [5] Z.Q. Shi, Y.J. Niu, Q. Wang, L. Shi, H.C. Guo, Y. Liu, Y. Zhu, S.F. Liu, C. Liu, X. Chen, R. Zhang, *J. Hazard. Mater.*, 2015, 298, 310.
- [6] G.E. Schaumann, A. Philippe, M. Bundschuh, G. Metreveli, S. Klitzke, D. Rakcheev, A. Grün, S.K. Kumahor, M. Kühn, T. Baumann, F. Lang, W. Manz, R. Schulz, H.J. Vogel, *Sci. Total Environ.*, 2015, 535, 3.
- [7] J.S. Lee, K.H. You, C.B. Park, *Adv. Mater.*, 2012, 24, 1084.
- [8] A. Bokare, A. Sanap, M. Pai, S. Sabharwal, A.A. Athawale, *Colloids. Surf. B: Biointerfaces*, 2013, 102, 273.
- [9] S.L. Mei, H.Y. Wang, W. Wang, L.P. Tong, H.B. Pan, C.S. Ruan, Q.L. Ma, M.Y. Liu, H.L. Yang, L. Zhang, Y.C. Cheng, Y.M. Zhang, L.Z. Zhao, P.K. Chu, *Biomaterials*, 2014, 35, 4255.
- [10] Z.J. Guo, C. Chen, Q. Gao, Y.B. Li, L. Zhang, *Mater. Lett.*, 2014, 137, 464.
- [11] K. Chaloupka, Y. Malam, A.M. Seifalian, *Trends Biotechnol.*, 2010, 28, 580.
- [12] K. Kamaraj, R.P. George, B. Anandkumar, N. Parvathavarthini, U. K. Mudali, *Bioelectrochemistry*, 2015, 106, 290.
- [13] S.M. Zacarias, M.L. Satuf, M.C. Vaccari, O.M. Alfano, *Chem. Eng. J.* 2015, 266, 133.
- [14] S.G. Mei, H.Y. Wang, W. Wang, L.P. Tong, H.B. Pan, C.S. Ruan, Q.L. Ma, M.Y. Liu, *Biomaterials*, 2014, 35, 4255.
- [15] Y.Q. Lin, L.B. Li, L.L. Hu, K.Y. Liu, Y.N. Xu, *Sens. Actuators B*, 2014, 202, 527.
- [16] Y.N. Chang, X. M. Ou, G. M. Zeng, J. L. Gong, *Appl. Surf. Sci.*, 2015, 15, 343.

- [17] M.F.Brugnera, M. Miyata, C.Q.F. Leite, M.V.B. Zanoni, J. Photochem. Photobiol., A: Chemistry, 2014, 278, 1.
- [18] A. Gao, R.Q. Hang, X.B. Huang, L.Z. Zhao, X.Y. Zhang, L. Wang, B. Tang, S.L. Ma, P.K. Chu, Biomaterials, 2014, 35, 4223.
- [19]C.J. Wu, G.X. Zhang, T. Xia, Z.N. Li, K. Zhao, Z.W. Deng, Mater. Sci. Eng. C, 2015, 55, 155.
- [20] W. Li, Z.Y. Ma, G.Q. Bai, J.M. Hu, X.H. Guo, B. Dai, X. Jia, Appl. Catal. B: Environmental, 2015, 43, 174.
- [21] Y.T. Yan, Q. Liu, X.J. Du, J. Qian, H.P. Mao, K. Wang, Anal. Chim. Acta, 2015, 853, 258.
- [22] L.Y. Wei, H.F. Wang, Z.Q. Wang, M.Y. Yu, S.G. Chen, RSC Adv.,2015,5, 74347.
- [23]W.Y. Gao, M.Q. Wang, C.X. Ran, X. Yao, H.H. Yang, J. Liu, D.L. He, J.B. Bai, Nanoscale, 2014, 6, 5498.
- [24]J.S. Chen, L. Xu, R.Q. Xing, J. Song, H.W. Song, D.L. Liu, J. Zhou, Electrochem. Commun., 2012, 20, 75.
- [25]G.X. Wang, X.J. Zhu, J.G. Yu, J. Power Sources, 2015, 278, 344.
- [26] H. Zhou, Y.F. Liu, W.D. Chi, C.Y. Yu, Y.J. Yu, Appl. Surf. Sci.,2013, 282, 181.
- [27] J. Zhu, Xi.Q. Liu, X.H. Wang, X.H. Huo, R. Yan, Sens. Actuators B, 2015, 21, 450.
- [28]Z. Shao, H.J. Li, M.J. Li, C.P. Li, C.Q. Qu, B.H. Yang, Energy, 2015, 87, 578.
- [29] W.C. Ye, X.Z. Shi, J. Su, Y. Chen, J.J. Fu, X.J. Zhao, F. Zhou, C.M. Wang, D.S. Xue, Appl. Catal., B: Environmental, 2014, 160-161, 400.
- [30] Y. Liao, Y.Q. Wang, X.X. Feng, W.C. Wang, F.J. Xu, L.Q. Zhang, Mater. Chem. Phys., 2010, 121,534.
- [31]L. Yu, X.F. Yang, Y.S. Ye, X.J. Peng, D.S. Wang, J. Colloid. Interf. Sci., 2015, 453, 100.
- [32]H. Mao, J.C. Liang, H.F. Zhang, Q. Pei, D.L. Liu, S.Y. Wu, Y. Zhang, X.M. Song, Biosens. Bioelectron., 2015, 70-15, 289.
- [33] Z.W. Zhao, J.X. Li, T. Wen, C.C. Shen, X.K. Wang, A.W. Xua, Colloid. Surf. A: Physicochemical and Engineering Aspects, 2015, 482, 258.
- [34] W.C. Wang,Y. Jiang,S.P. Wen,L. Liu,L.Q. Zhang, J. Colloid. Interf. Scie., 2012, 368, 241.
- [35]B. Lepoittevin, S.Bedel, D. Dragoé, J. Bruzaud,M. Geneviève, B. Labrousse, S. Mazerat, J.M. Herry, M.N.B. Fontaine, P. Roger, Prog. Org. Coat., 2015, 82, 17.
- [36] J. Xiong, X.D. Wu, Q.J. Xue, Colloid. Surf. A: Physicochem. Eng. Aspects, 2013, 423 , 89.
- [37] T. Li, O.L. Lin, Z.Y. Lu, L.M. He, X.S. Wang, Appl. Surf. Sci., 2014, 305, 386.
- [38] C.J. Wu, G.X. Zhang, T. Xia, Z.N. Li, K. Zhao, Z.W. Deng,Di.Z. Guo, B. Peng, Mater. Sci. Eng. C, 2015, 55, 155.
- [39] S. Calderon V., R. Escobar Galindo, J.C. Oliveira, A. Cavaleiro, S. Carvalho, Surf. Coati. Tech., 2013, 222, 104.
- [40] R. Goei, T.T. Lim, Water Res., 2014, 59, 207.
- [41] Duangkamon Jiraroj, Sukkaneste Tungasmita, Duangamol N. Tungasmita, Powder Technol., 2014, 264, 418.
- [42] N. Joshia, B.T. Ngwenya, I.B. Butler, C.E. French, J. Hazard. Mater., 2015, 287, 51.
- [43] A. Bokare, A. Sanap, M. Pai, S. Sabharwal, A.A. Athawale, Colloid. Sur. B: Biointerfaces, 2013, 102, 273.

## Graphical abstract

